

Status of black-hole-binary simulations for gravitational-wave detection

Mark Hannam

Physics Department, University College Cork, Cork, Ireland

Abstract. It is now possible to theoretically calculate the gravitational-wave signal from the inspiral, merger and ringdown of a black-hole-binary system. The late inspiral, merger and ringdown can be calculated in full general relativity using numerical methods. The numerical waveforms can then be either stitched to inspiral waveforms predicted by approximation techniques (in particular post-Newtonian calculations) that start at an arbitrarily low frequency, or used to calibrate free parameters in analytic models of the full waveforms. In this review I summarize the status of numerical-relativity (NR) waveforms that include at least ten cycles of the dominant mode of the GW signal before merger, which should be long enough to produce accurate, complete waveforms for GW observations.

PACS numbers: 04.20.Ex, 04.25.Dm, 04.30.Db, 95.30.Sf, 04.25.Nx, 04.30.-w

1. Introduction and overview

A worldwide network of detectors [1, 2, 3] is poised to make the first direct observation of gravitational waves (GWs). Gravity is the weakest of the fundamental forces, and even GWs produced by the collision of two black holes — one of the most likely sources for the first detection — will produce a signal obscured by detector noise; signal-to-noise ratios (SNRs) less than ten may be typical. One way to locate the signal is to compare the detector data against a collection (template bank) of the signals predicted by Einstein’s general theory of relativity for a range of potential sources. In the case of black-hole-binary mergers, the only way to calculate the signals predicted by the full theory is to solve Einstein’s equations on a computer.

Numerical solutions of Einstein’s equations for the last orbits and merger of a black-hole binary, the ringdown of the single black hole that remains, and the GWs emitted in the process, became possible in 2005 [4, 5, 6]. Since that time many simulations have been performed, producing results relevant to mathematical general relativity, black-hole physics, and galactic astrophysics. In this article, however, I review the status of black-hole-binary simulations for the purpose of GW detection.

Consider the archetypal black-hole-binary configuration studied in a numerical simulation: two black holes of equal mass, with no spin, in orbit with zero eccentricity. If the two black holes orbit with a frequency $\Omega(t)$, then the frequency of the dominant GW mode is $\omega(t) \approx 2\Omega(t)$. As GWs are emitted, the black holes spiral slowly inwards, and the GW frequency increases; so too does the GW amplitude, $A(t)$. The rate of inspiral grows, and the GW frequency and amplitude sweep up until the two black holes plunge together and merge, at which time the GW amplitude peaks and then decays exponentially, while the frequency levels off at the ringdown frequency of the

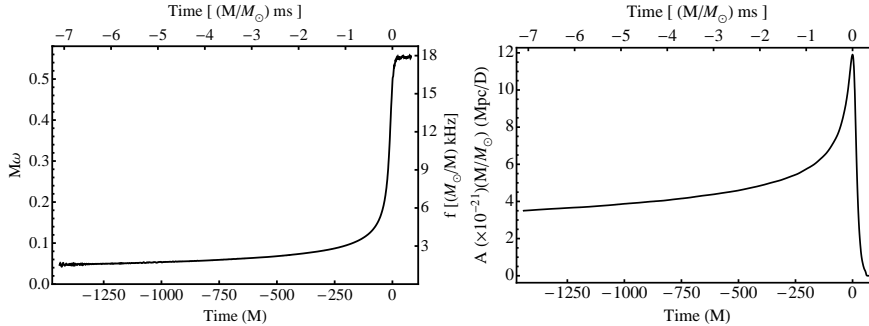


Figure 1. Frequency and amplitude of the GW signal from a numerical simulation of the last eight orbits, merger and ringdown of an equal-mass nonspinning binary. The amplitude is given for an optimally-oriented binary. The time is given in units of the total mass M of the binary, and in milliseconds. The frequency is in dimensionless units $M\omega$ and kHz. The amplitude of the GW strain $\Delta L/L$ is dimensionless and scales with respect to the binary's mass M and distance D (in megaparsecs) from the detector. (Data from high-resolution D12 simulation used in [7].)

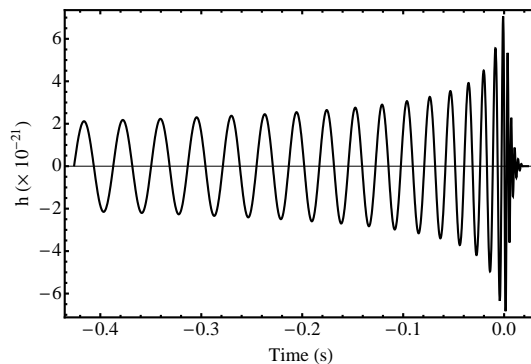


Figure 2. The full GW strain signal for the same configuration as in Fig. 1, for a $60 M_{\odot}$ binary located 100 Mpc from the detector.

remnant Kerr black hole. This behaviour is illustrated in Fig. 1 for the last sixteen cycles (eight orbits) and merger and ringdown from a numerical simulation of an equal-mass nonspinning binary. The time is shown both in units of the total mass M of the binary (which is an overall scale factor for the numerical solution), and the corresponding time in milliseconds for binaries with the total mass as some multiple of the mass of the sun, $M_{\odot} = 1.477 \times 10^3 m$. As an example of a complete waveform, Fig. 2 shows the wave strain $h(t) = \Delta L(t)/L$ from a $60 M_{\odot}$ binary located 100 Mpc away and optimally oriented to the detector.

Now consider the Enhanced LIGO detectors, which are scheduled to begin a science run in mid-2009 [8]. They are sensitive to signals with frequencies higher than ≈ 30 Hz. The signal as represented in Figs. 1 and 2 could therefore be detected from roughly the point where the frequency sweeps through 30 Hz; at lower frequencies the detector noise completely swamps the signal. We see that the point at which the signal enters the detector band depends on the binary's total mass. If the mass is too high ($\geq 600 M_{\odot}$), the final ringdown frequency will be below 30 Hz and the signal will never

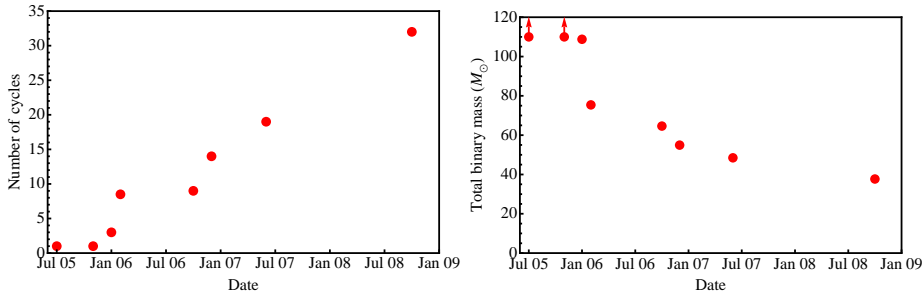


Figure 3. An indication of the development of numerical simulations since the first simulations in 2005. The first panel shows the number of GW cycles before merger of an equal-mass nonspinning binary. The second panel shows the minimum total mass of binaries that could be searched for in Initial or Enhanced LIGO data with these waveforms; for the two points with arrows, the minimum detectable total mass is $M \approx 380M_{\odot}$. See text for further details.

enter the detector’s sensitivity band. If the mass is too low, then the detector will see much more of the waveform than shown in Figs. 1 and 2. In that case this numerical waveform will describe only *part* of the detected waveform, and will therefore not be the optimal theoretical waveform to use in a GW search. We see then that the usefulness of a waveform depends on its length; if an NR waveform has a starting frequency of $M\omega_i$ (a dimensionless quantity calculated from the simulation), and a detector has a low-frequency limit of f_0 , then the waveform is best suited to search for binaries with masses $M/M_{\odot} \gtrsim 32300\omega_i/f_0$. For the Enhanced LIGO detector, with $f_0 \approx 30$ Hz, we can search for binaries with masses $M/M_{\odot} \gtrsim 1076 (M\omega_i)$. Note also that if the mass is very low ($\sim 1 M_{\odot}$), then the merger and ringdown will occur at frequencies *too high* to be detected, and only the inspiral will be visible.

With this discussion in mind, Fig. 3 demonstrates the progress of NR simulations to date, for the default case of an equal-mass nonspinning binary following (ideally) non-eccentric inspiral. The first published simulations in 2005 covered only half an orbit, or one GW cycle, before merger [4, 5, 6]. The first panel of Fig. 3 shows the number of cycles covered by successive simulations of the same system [9, 10, 11, 12, 7, 13]. The dramatic progress is clear: in three-and-a-half years the number of cycles increased from one to more than thirty. What is not shown in this plot is that the accuracy of the simulations also improved: gravitational waves were extracted with greater precision, the binary’s eccentricity was significantly reduced, and the phase error in the waveforms dropped by several orders of magnitude. (I will discuss waveform accuracy in Sec. 3.) The purpose of this figure is not to suggest that progress will continue in the same way — in fact, it is unlikely that anyone will attempt to produce an even longer simulation of this configuration until the appearance of a new generation of numerical methods — but simply to illustrate the rate of progress since July 2005.

A less optimistic picture from the point of view of GW detection is given in the second panel of Fig. 3, which shows the lowest-mass binary that we could search for with these waveforms, based on the discussion above. For the first simulations, $M\omega_i = 0.356$ [5], and the resulting waveforms were therefore appropriate for searches in Enhanced LIGO data for binaries with $M \gtrsim 383 M_{\odot}$; the two data points that represent these waveforms [9, 10] are off the scale of the plot. In three-and-a-half

Table 1. Black-hole-binary configurations for which numerical waveforms exist, and which include at least ten GW cycles before merger.

Configuration	Cases	Cycles	Reference
Equal mass			
Nonspinning	$e \sim 0$	Up to 32	[12, 7, 13].
Nonspinning	$e \sim 0.1, 0.2, 0.3$	12 – 21	[16, 17]
Equal parallel spins	$ a/m \leq 0.925$	Up to 20	[15, 18]
Unequal mass			
Nonspinning ($q = M_1/M_2$)	$q \leq 6$	12 – 20	[19, 20, 21]
Precessing spins	$a/m \sim (0.6, 0.4)$	≈ 20	[22]

years the low-mass limit has improved by an order of magnitude to just below $40 M_\odot$. However, we also see that the decrease in the lower mass limit does not fall in proportion to the increase in cycles. This is because the GW frequency increases very slowly during the inspiral, until a few cycles before merger. If we want a waveform that can detect binaries with total masses below, for example, five solar masses, we will need waveforms that are not just eight times longer than the last point in Fig. 3 [13], but hundreds of times longer. This is a serious problem, because the most likely sources for the first detection of GWs are predicted to have masses lower than $50 M_\odot$ [14].

Figure 3 suggests that at some point it becomes computationally inefficient to produce increasingly longer simulations. How then are we to produce templates to detect low-mass binaries? One way is to connect an NR waveform for the last orbits and merger to a long inspiral waveform predicted by the post-Newtonian (PN) approximation — *if* the PN waveform is accurate enough. I discuss the validation of PN waveforms by comparison with full GR numerical waveforms in Sec. 4, and the construction of hybrid PN-NR waveforms in Sec. 5. Hybrid waveforms can in principle be used to detect binaries of any mass, within the limits of a given detector.

This does not solve the problem of producing all the waveforms necessary to search for GWs from black-hole binaries, because we have considered only one configuration: an equal-mass nonspinning binary with (ideally) zero eccentricity. The parameter space of black-hole binaries is far larger. It includes the mass ratio $q = M_1/M_2$ of the two black holes, their spins \mathbf{S}_1 and \mathbf{S}_2 , and the binary’s eccentricity, e .

Table 1 summarizes the sections of this parameter space that have been covered by simulations to date. Keeping in mind the ultimate goal of producing hybrid waveforms (or other forms of complete waveform; see Sec. 5), I focus only on simulations that include more than ten GW cycles (about five binary orbits) before merger. This summary should serve as a quick reference of the status of simulations useful for GW detection. It may turn out that shorter waveforms are sufficient to produce detection templates, or conversely that they need to be much longer. The choice of ten orbits seemed a reasonable limit based on PN-NR comparisons to date (see for example [7, 15]), and also manages fairly successfully to separate out those simulations that were performed with GW observation applications as the primary motivation.

Having provided this broad overview, I will now turn to the details of producing NR waveforms, and current efforts to make them useful for GW observations. Section 2 summarizes what I consider to be the most relevant details of current numerical methods: computational issues, black-hole-binary initial data, evolution systems, and gravitational-wave extraction. More details on these topics can be found in [23, 24]. Section 3.1 addresses the physical and numerical accuracy of simulations and the

consistency between results from different codes. With the production of complete waveforms in mind, Sec. 4 discusses work on comparing PN results with full GR. Section 5 is devoted to methods to construct complete waveforms and families of waveforms for template banks. In Sec. 6 I highlight a number of issues for future numerical simulations and their use for GW observations.

2. Production of numerical waveforms

In this section I will briefly summarize current techniques to numerically solve Einstein’s equations for a black-hole-binary spacetime.

2.1. Length scales and computational resources

The defining length scale of a simulation is some measure of the total mass M of the physical system. This is either chosen as the sum of the black-hole masses, $M = M_1 + M_2$, or the total (Arnowitt-Deser-Misner, or ADM) energy of the spacetime, $M = M_{ADM}$. The difference between the two measures is small, and is often referred to as the binding energy of the binary. The length scale M is then used to characterize all measures in a simulation; a simulation may for example consider two black holes each with mass $M/2$, initially $10M$ apart, which evolve for about $1000M$ before merging, and emitting gravitational waves that are calculated $100M$ from the binary’s center of mass. This overall scaling with M means that we can use one simulation to describe the waveform from a binary of any mass.

To accurately simulate a black-hole-binary spacetime, a computer code must adequately resolve both the region near the black hole, and the spacetime far away, where gravitational waves are extracted. In the codes used to produce the results I will discuss here, resolutions of at least about $M/16$ are needed near the black holes. By contrast, the wavelength of the dominant mode of the gravitational waveform is on the order of $10M$ during the merger phase, and so resolutions on the order of $\sim M$ are needed in the region where gravitational waves are extracted, which can be as far as several hundred M from the binary. To deal with such large differences in resolution requirements on different parts of the computational domain many codes use mesh refinement methods [25]. Another technique is to use a coordinate transformation that changes the effective resolution in different regions; such a “fisheye” transformation was used in early results from the `LazEv` code [5, 9, 26, 27, 28], and was also used in more recent simulations by the UIUC group, for example [29]. A third option is to divide the computational domain into a number of different domains or patches, and use a different numerical resolution and even different coordinate systems in each domain; a multi-domain method is used in the `SpEC` code [30]. The problem of length scales becomes even greater when we consider the sub-dominant modes of the GW signal, which are both weaker and have wavelengths much smaller than the dominant mode; for example, if we consider modes up to $\ell = 6$, then the $(\ell = 6, m = 6)$ mode will have a wavelength one third of the length of the dominant $(\ell = 2, m = 2)$ mode, and the amplitude may be several orders of magnitude smaller.

Ideally the outer boundary of the computational domain is located at spatial or null infinity. The only long-term binary evolution code where one of these techniques is employed is that of Pretorius, where spatially compactified coordinates are used [31, 4]. The region near the outer boundary is by definition poorly resolved, but a filtered buffer zone between the well- and poorly-resolved regions is used to reduce the build-

up and propagation of any resulting errors. In all other codes the outer boundary of the computational domain is not at spatial infinity, and boundary conditions must be imposed. The physically correct outer boundary conditions are not known for a black-hole-binary spacetime, and approximate boundary conditions must be used. The BSSN codes generally use Sommerfeld-like outer boundary conditions (which are physically correct only for a spherically symmetric wave pulse on a flat background), and the outer boundary is placed as far from the binary system as computational resources allow, typically on the order of $\sim 1000M$. The effect of the outer boundary errors on the predicted GW signal (extracted at $\sim 100M$) is small, and is usually estimated as comparable or smaller than other error sources in the code. The Caltech-Cornell SpEC code uses a set of constraint-preserving boundary conditions [32] that provide a far better approximation to the correct physics of outgoing waves on a dynamical spacetime than Sommerfeld conditions, and make it possible to place the outer boundary at $< 1000M$ and still achieve accurate results [33].

These simulations require large computational resources. Long black-hole-binary simulations are typically run on multiple processors of a supercomputer, and we can get an impression of the “size” of a simulation from the amount of memory it requires, and the number of CPU hours it takes to run. I did not include computational costs in Tab. 1 because they are not always published. As an example, however, the highest-accuracy equal-mass nonspinning waveform produced in [7] took roughly 18 days running on 24 processors, for a total of about 10,000 CPU hours.

The reader interested in the technical details of the codes currently in use, and how they differ, is referred to Section 2 of [34] as a useful starting point.

2.2. Initial data

Astrophysical black holes ultimately form through gravitational collapse of matter, but in a black-hole simulation one need not describe the matter at all. The black hole can instead be represented purely through its effect on the spacetime geometry. The spacetime singularity at the center of a black hole is difficult to describe numerically, and there are two approaches to this problem. One is to terminate the computational domain before it reaches a singularity; this is called “excision” of the black hole [35]. No information can escape a black hole, and so the rest of the spacetime is unaware that the black-hole interior is missing from the numerical solution. In practice excision is not as simple as it sounds: we must specify appropriate boundary conditions on the excision surface, and we must ensure that the numerical representation of the Einstein equations respect the speed-of-light limit on information propagation; although physical information cannot escape the black-hole, non-physical numerical or gauge information can in principle escape, and may lead to numerical instabilities. Excision is used in Pretorius’s code [31, 4, 36], and in the SpEC code [30].

Pretorius’s original simulations began with scalar-field initial data, chosen such that it would quickly collapse to form a black hole. Once the black hole had formed, the interior (and the remaining scalar field) were excised. Some of his later simulations, as well as those performed with the SpEC code, used excision data generated by solving the conformal-thin-sandwich formulation [37, 38] of the initial-value equations of general relativity, subject to inner boundary conditions that lead to either co-rotating or irrotational black holes, and outer boundary conditions that effectively specified the orbital speed of the binary [39, 40, 41].

The second method of avoiding singularities is to choose coordinates that bypass

them: the black holes are initially described with topological wormholes, such that as the numerical coordinates approach one of the black holes, they pass through a wormhole and instead of getting closer to the singularity end up further away, in a new asymptotically flat region. A coordinate transformation is performed to compactify these wormholes, and the extra asymptotically flat regions are reduced to single points, called punctures [42, 43, 44, 45]. Alternatively one may choose “trumpet” coordinates such that as we approach the black hole, we find that we are getting no closer to the singularity, but are instead following an infinitely long cylinder [46]. These cylinders, or trumpets, can also be compactified to punctures, and in fact this is the representation of the black holes that simulations that start with wormhole-puncture initial data “naturally” evolve towards [47, 48, 49, 46].

All of the initial data used to produce the waveforms I will discuss are conformally flat, meaning that the spatial metric on the initial slice γ_{ij} is related to the flat metric δ_{ij} by a conformal factor ψ as $\gamma_{ij} = \psi^4 \delta_{ij}$. A spacetime that contains an orbiting black-hole binary will not be conformally flat, even if we neglect the gravitational-wave content. The use of conformal flatness simplifies the construction of the initial data, but leads to a burst of junk radiation as the black holes settle down to “true” boosted Schwarzschild or Kerr black holes. The junk radiation quickly leaves the system, and does not seem to adversely affect the physics. However, the use of conformal flatness places an effective limit on the spin of each black hole of $a/m \lesssim 0.93$ [50], and the junk radiation severely limits the accuracy of simulations of black holes boosted to highly relativistic speeds [51, 52]. Approaches to move beyond conformal flatness have been proposed for both excision [53, 54, 55, 56, 57, 58, 59] and puncture data [60, 52, 61], although they have not yet been used for the long-term orbit simulations of the kind we are focussing on here.

2.3. Evolution systems

Given black-hole-binary initial data, a stable evolution requires a numerically well-posed and stable formulation of Einstein’s equations, as well as a judicious choice of gauge conditions. Finding a suitable set of evolution equations and gauge conditions was one of the major problems in the field during the decade preceding the 2005 breakthroughs. The textbook [23] contains a review of this topic, and the mathematical issues are discussed further in [62, 63]; and one illustration of the severity of the problems is the Apples with Apples project [64, 65].

Although not all mathematical and numerical questions have been resolved, long-term stable simulations can now be performed with either a variant of the generalized harmonic formulation [66, 62, 31, 67] or the moving-puncture treatment [5, 6] of the Baumgarte-Shapiro-Shibata-Nakamura (BSSN) [68, 69] formulation. A review of successful methods and applications for black-hole-binary simulations is given in [24].

The generalized harmonic formulation deals directly with the full spacetime metric, $g_{\mu\nu}$. The metric evolves via a set of generalized wave equations, which are in a manifestly hyperbolic form. In standard harmonic coordinates, the spacetime coordinates x^μ are chosen to satisfy $\square x^\mu = 0$. This condition is now generalized so that the gauge (coordinate) conditions are specified by source functions $\square x^\mu = H^\mu$ [66, 62, 31], which in turn are either specified functions of time, or satisfy their own evolution equations [4, 36, 33, 70, 13].

The BSSN decomposition starts instead with the (numerically ill-posed) ADM-York equations for the spatial quantities (γ_{ij}, K_{ij}) [71, 72]. The BSSN reformulation

provides evolution equations for conformally rescaled quantities, $\{\psi, K, \tilde{\gamma}_{ij}, \tilde{A}_{ij}, \tilde{\Gamma}^i\}$, where $\gamma_{ij} = \psi^4 \tilde{\gamma}_{ij}$ and $K_{ij} = \psi^4 (\tilde{A}_{ij} + \tilde{\gamma}_{ij} K)$, and the extra variable, $\tilde{\Gamma}^i = \partial_j \tilde{\gamma}^{ij}$ is introduced. The moving-puncture extension of the BSSN system deals with puncture data, and involves introducing either $\phi = \ln \psi$ [6], $\chi = \psi^{-4}$ [5] or $W = \psi^{-2}$ [73], and evolving that quantity instead of the conformal factor ψ , and specifying gauge conditions that allow the punctures to move across the numerical grid. Although developed heuristically over time, these gauge conditions serendipitously attract the numerical slices to approximate stationarity (so that the variables evolve largely due to the physics, and not mere coordinate changes), and move the punctures across the grid. The behaviour of these gauge conditions for moving-puncture evolutions of a Schwarzschild black hole are discussed in detail in [46]. The numerical stability of the moving-puncture system is considered in [74, 75].

The generalized-harmonic and moving-puncture methods have been found to work for simulations of up to 15 orbits, for binaries with significant eccentricity, with mass ratios up to 1:10, and spins up to the conformal-flatness limit of $a/m \sim 0.93$. Despite this wealth of evidence that these methods work, surprisingly little has been done to explain why. The properties that are known to be necessary for a stable simulation (in particular, a symmetric hyperbolic evolution system), are also known to not be sufficient. What distinguishes these methods from others? Could it be that most other (well-posed) systems of equations can be stably evolved with appropriate gauge conditions and methods to move the black holes through the grid? Are there situations where the current methods will fail? These questions have been largely neglected, and deserve more attention.

2.4. Gravitational-wave extraction

Finally, once we have evolved a black-hole-binary system through its last orbits, merger and ringdown, we want to measure the gravitational-wave signal that was emitted. This is done by calculating either the Newman-Penrose scalar Ψ_4 [76, 77], which is a measure of the outgoing transverse gravitational radiation in an asymptotically flat spacetime, or the odd- and even-parity master functions Q^+ and Q^\times in the Zerilli-Moncrief formalism (see [78] for a review). The wave strain, $\mathbf{h} = h_+ - ih_\times$, is related to Ψ_4 by two time integrations, and to $Q^{+, \times}$ by one time integration. The quantities are calculated on spheres of constant coordinate radius some distance from the binary, and then decomposed in spin-weight $s = -2$ spherical harmonics ${}_s Y_{\ell m}$. Not only are the (ℓ, m) harmonics more easily compared with analytic predictions of the GW signal, which are usually presented in the same way, but calculating the contribution to each mode involves an integration over the entire sphere,

$$\mathbf{h}_{\ell m} \equiv \langle {}_{-2} Y_{\ell m}, \mathbf{h} \rangle = \int_0^{2\pi} d\phi \int_0^\pi \mathbf{h} {}_{-2} \bar{Y}_{\ell m} \sin \theta d\theta, \quad (1)$$

which effectively smooths out numerical noise; for example, Ψ_4 calculated at one point on the numerical grid is typically rather noisy, while Ψ_4 reconstructed from a (reasonable) number of modes will be a clean wave signal. Given the values of the spherical harmonics, the corresponding wave signal can be calculated for any sky location and binary orientation.

Producing the strain \mathbf{h} from Ψ_4 appears at first sight to be merely a matter of performing two time integrations of Ψ_4 and appropriately choosing two integration

constants. However, the numerical data contain numerical noise, and also small deviations from the “correct” signal that would be seen at infinity due to gauge effects. These small errors can be grossly magnified after an integration over the entire duration of the waveform, and producing h from Ψ_4 requires *two* such integrations. One may be tempted to first Fourier transform Ψ_4 to the frequency domain, where two time integrations can be trivially performed, but this also involves an implicit choice of integration constants, and once again care has to be taken to produce physically reasonable results (see for example [22]).

The gauge errors in Ψ_4 will decay with increasing extraction radius — or at least they will with an appropriate gauge choice [79], which seems to be the case with typical gauge choices [7, 33, 13]; the good agreement between results from both the Newman-Penrose and Zerilli-Moncrief methods provides further evidence that our gauges are well-behaved [80]. This suggests that we can try to reduce gauge errors by extrapolating the waveform to an estimate of the wave that would be observed at infinity (i.e., by a distant detector). Unfortunately the extrapolation is rarely perfectly clean, and introduces further numerical noise that tends to produce an even less believable version of the strain than an integration based on the raw data.

Despite these difficulties, one may produce a reasonable estimate of the strain by applying a number of “cleaning” procedures; see, for example [81]. An alternative option, of course, is to calculate $Q_{\ell m}^+$ and $Q_{\ell m}^\times$ instead, from which the strain can be produced by only one time integration, and the results are in general far cleaner.

3. Reliability of numerical waveforms

Before using NR waveforms for GW applications, we need to quantify their numerical and physical accuracy. We also need to verify that the results produced with different sets of evolution equations, initial-data, gauge conditions and wave extraction methods are all consistent.

3.1. Numerical and physical accuracy

One of the most important checks of a numerical result is a convergence test. A given numerical method will be expected to converge to the continuum solution as some function of the numerical resolution. For example, if a method to solve a one-dimensional problem to find a solution $f(x)$ is second-order accurate in the grid spacing Δx , then the numerical solution $\bar{f}(x)$ will be related to the true solution $f(x)$ by

$$f(x) = \bar{f}(x) + a(x)\Delta x^2 + \mathcal{O}(\Delta x^3). \quad (2)$$

In this case, each time we halve the grid-spacing Δx , the error in the solution should decrease by roughly a factor of four. If we have an analytic solution to compare with, we can readily verify the dependence of the error on the grid spacing, and if not we look instead at $f_{\Delta x}(x) - f_{\Delta x/2}(x)$ for several choices of Δx . A convergence test verifies that the code is producing a valid solution of a system of partial difference equations, and helps determine how much numerical resolution is required for the code to be in the convergent regime and for the solution to be sufficiently accurate.

In large and complex codes like those used to simulate black-hole-binary systems, convergence tests are rarely as straightforward as suggested above. In a mesh-refinement-based code, different parts of the code may have different theoretical convergence orders, and it may be far from clear how the overall convergence should

behave. Ultimately one should be able to choose a high-enough resolution such that the lowest-order part of the code dominates. However, 3D numerical simulations require large computational resources, and successively halving the grid spacing until the predicted convergence rate is seen is usually not practical. Simulations are often performed at the edge (or what is perceived to be the edge) of the convergent regime, and convergence behaviour deemed sufficiently close to theoretical expectations is usually considered acceptable. The definitions of “sufficiently close” and “acceptable” are of course subjective, but in most cases the error estimates quoted in the literature err on the side of caution. Those who remain suspicious may be reassured by Section 3.2 below.

The uncertainties and errors in a numerical waveform are not defined entirely by the convergence properties of the code. There are also errors in the physical specification of the data. The definition of black-hole mass (used to define the overall scale of the simulation) is not unique, nor is the measurement of black-hole spins. A simulation that is supposed to model non-eccentric inspiral will always have some remaining eccentricity, and for eccentric binaries there is (once again) no unique definition of eccentricity. (Zero eccentricity is relatively easy to define; it’s just difficult to achieve [82, 83, 33, 22, 84]) Finally, and often most importantly, we want the gravitational-wave signal as measured far from the source, in the region where the wave can be considered as a perturbation on flat space. In practice the waves are extracted from the numerical solution only a few hundred M from the source; for a binary that consists of two solar-mass black holes, this is equivalent to measuring the gravitational waves only about 300 km away, about one hundred-millionth of the distance of the Sun to the Earth! As ridiculous as this may sound, it is a large enough distance in general relativistic terms that the amplitude error in a numerical waveform is only a few percent — it should simply be borne in mind that this few-percent error may be the largest error ingredient in the entire waveform. A good illustration of the errors that enter into the calculation of a numerical waveform are provided in Table III of [33].

Both the numerical and physical accuracy of numerical waveforms has improved steadily since 2005. The first simulations were performed with a code that resolved each time slice with second-order-accurate finite differences [4]. The moving-puncture results that followed six months later [5, 6] used second- and fourth-order-accurate finite differences. An accurate comparison of numerical and post-Newtonian waveforms was performed in 2007 using sixth-order finite-differencing [85, 7], and the **LazEv** code now routinely uses eighth-order methods [86]. The **SpEC** code, which has produced the most accurate equal-mass nonspinning binary waveform to date, uses pseudospectral methods to describe the spatial slice, and achieves an overall error in the phase during 30 cycles of inspiral, merger and ringdown of less than 0.1 radian, and an uncertainty in the amplitude of at worst (during merger and ringdown) of 1% [33, 13].

3.2. Consistency between solutions

The uncertainty estimates published with numerical waveforms lead us to believe that those waveforms are extremely accurate. However, these solutions were produced using different formulations of Einstein’s equations, different numerical methods and, perhaps more importantly, different gauge conditions, families of initial data and wave extraction methods. The effects of these different approaches, although they

are expected to be small, need to be fully quantified.

With this goal in mind a comparison was performed between three of the early black-hole-binary simulations in 2006 [87]. Since then many much longer simulations have been performed with far greater accuracy, and it is these more recent simulations that are likely to play a role in future GW searches; some have already been used for the NINJA project [34] to test GW search pipelines on NR waveforms buried in simulated detector noise. As such, a project to compare long waveforms in the context of GW data analysis has been organized as a complement to the NINJA project, and has been dubbed Samurai [88].

The Samurai project compares equal-mass nonspinning waveforms from five codes, dealing with only the last $1000M$ before merger, and $80M$ after merger. The five codes are `BAM` [89, 90], `CCATIE` [91], `Hahndol` [92, 74], `MayaKranc` [93] and `SpEC` [94]. Since the `SpEC` waveform has the lowest associated numerical uncertainties, it is used as the reference against which the others are compared.

Two kinds of comparison are performed. The first deals with the phase and amplitude agreement of the Ψ_4 waveforms. It is found that all of the waveforms agree within their claimed internal uncertainty. This acts as a clear validation of the results between different codes, and demonstrates that the variation between waveforms due to different numerical techniques, initial data, gauge conditions and wave-extraction methods is at worst no larger than the internal error estimates in each waveform.

The details of the uncertainties in each numerical code are of little direct interest in the practical business of GW detection and source parameter estimation. For that reason a second comparison attempts to assess what the apparently small differences between the five waveforms mean for GW searches. The relevant quantity to compare for GW detection is the match \mathcal{M} between two waveforms, which quantifies their disagreement with respect to the noise spectrum of a given detector [95]. In GW searches, if the match between the correct physical waveform and the template is greater than 0.965, then no more than about 10% of signals will be lost.

For the Samurai waveforms, the matches are so close to unity that it makes more sense to consider the mismatch, $1 - \mathcal{M}$. Figure 4 shows the mismatch between the `SpEC` waveform and the others for the Enhanced LIGO and Virgo detectors. (The lower mass cut-off for each plot is determined by the calculation discussed in the Introduction; the low-frequency limit for Virgo is taken as 10 Hz.) As is clear from the figure, the matches are well within the standard $1 - \mathcal{M} < 0.035$ threshold for detection!

One can also make a comparison relevant to parameter estimation. As discussed in [96], if the signal-to-noise ratio of the difference between two waveforms $\delta\mathbf{h}(t) = \mathbf{h}_1(t) - \mathbf{h}_2(t)$ is less than one, then the two waveforms will be indistinguishable in a GW search. The SNR of both the waveforms and their difference decreases in inverse proportion to the distance D of the detector from the source. We can therefore determine the maximum SNR such that, if a signal were detected with a lower SNR, it would not be possible to distinguish whether it was \mathbf{h}_1 or \mathbf{h}_2 . For the Enhanced LIGO and Virgo detectors, a detection will be considered reliable if the SNR is above 5–8, and SNRs above 30 are considered unlikely. (For example, the maximum SNR of injections for the NINJA project is 30 [34].)

Figure 5 shows the maximum SNR for indistinguishability for the Samurai waveforms. The measurement criteria was minimized over a time- and phase-shift, so these results do not apply to a measurement of the time of arrival or initial phase of the waveform, or any parameter that is affected by them (for example the sky location),

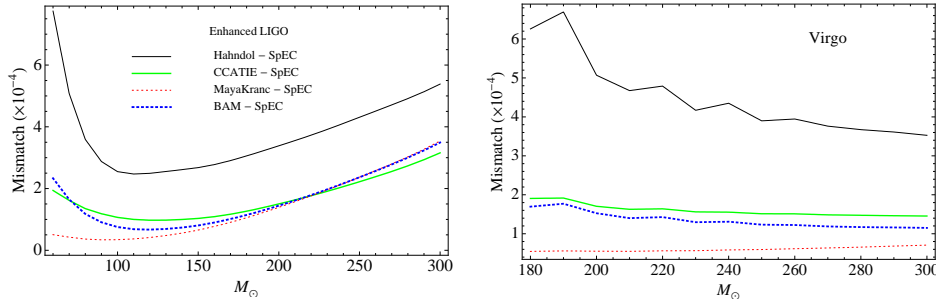


Figure 4. The mismatch between the SpEC waveform and each of the other codes. The two plots show the results for the Enhanced LIGO and Virgo noise curves. The lower end of the mass range was chosen such that the entire numerical waveform was included in the detector’s frequency band. (Plot taken from [88].)

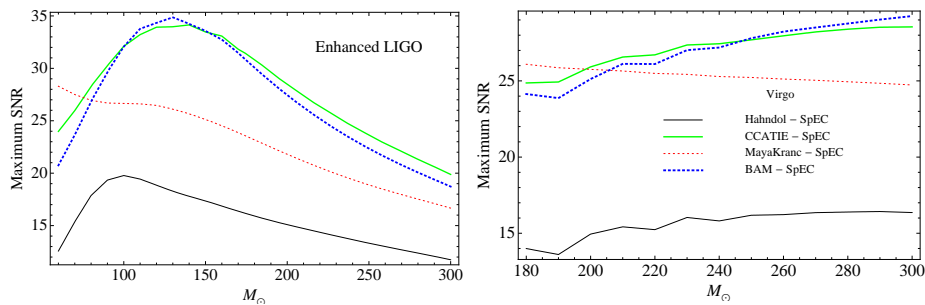


Figure 5. The signal-to-noise ratio (SNR) for which the SpEC and each other waveform will be indistinguishable in any measurement of intrinsic parameters. Results are shown for the Enhanced LIGO and Virgo detectors. See text for further explanation. (Plot taken from [88].)

but it *does* apply to any of the intrinsic parameters of the binary $\{M, q, \mathbf{S}_1, \mathbf{S}_2, e\}$ that we first discussed in Sec. 1; this simple analysis is also limited to single-detector searches. Within these caveats, and within the range of binary masses shown in Fig. 5, we see that in general the signals are indistinguishable for an SNR below about 25, and in all cases cannot be distinguished if the SNR is below ~ 14 . This suggests that these five waveforms are unlikely to be distinguishable (for intrinsic parameters) in single detectors prior to the commissioning of Advanced LIGO and Virgo in 2014. A comparable study remains to be done for unequal-mass binaries with precessing spins, which are computationally more challenging to simulate, but recent first long simulations of such systems [22] suggest that similar levels of accuracy are possible. As such we expect that the current level of accuracy and consistency of numerical waveforms is adequate for at least the next five years.

Beyond that time, it is important to bear in mind that these results refer to only the dominant mode of the GW signal. The subdominant modes are unlikely to change the results for GW detection (although this depends on the orientation of the binary), but can be important for parameter estimation [97, 98]. Since the Samurai results suggest that the black-hole dynamics are captured accurately in current simulations, achieving comparable accuracy of the higher modes depends only on the accuracy of the wave extraction (the distance of extraction from the source, and the numerical

resolution in the wave-extraction zone), and suggest that this is where efforts should be directed in improving numerical simulations; I will say more about this in Sec. 6.

Having concluded that numerical waveforms are in general sufficiently accurate for use in data-analysis applications, we move on to the question of providing waveforms of arbitrary length.

4. Comparison with post-Newtonian predictions

As we saw in the Introduction, current waveforms can only be used to search for binaries with total masses above $\sim 40 M_\odot$, and waveforms suitable for searches of binaries with masses below $5 M_\odot$ would need to be hundreds or thousands of times longer. (References to the binary’s mass will always be to the *total* mass of the binary, $M = M_1 + M_2$.)

Fortunately we do not need to simulate all of those orbits in full general relativity. The wave signal from the slow inspiral can also be modeled by post-Newtonian (PN) methods, and one would hope that the PN approximation is adequate up to the point where we begin our numerical simulations, and that it is possible to smoothly connect the PN and NR signals to produce a “complete” waveform. I will discuss work on producing such complete waveforms in Section 5. But first one must quantify the level of accuracy of the PN approximants.

Consider a $10 M_\odot$ equal-mass nonspinning binary. PN calculations tell us that the Enhanced LIGO sensitivity band will contain about 150 orbits (300 cycles) before merger, and the signal will last about 6.5 s. The first panel of Fig. 6 shows the frequency evolution after 6.45 s. Although the plot includes only 0.05 s of the 6.5-second-long signal, this accounts for around 20% of the power output of the entire signal; see Fig. 4 in [99]. The solid line shows the PN frequency as a function of time, and the dashed line shows the NR result. The PN line was produced with the TaylorT1 approximant, and was cut off just before it diverges. Similar results would be obtained with any other standard (i.e., Taylor-expanded) PN approximant; the figure was produced purely as an illustration of the general behaviour of PN and NR results. The second panel of Fig. 6 shows the corresponding time development of the amplitude of the ($\ell = 2, m = 2$) mode of the GW strain if the binary were optimally oriented to the detector and located 100 Mpc away. The PN and NR waveforms were aligned in time such that $M\omega = 0.1$ at the same time for each.

The PN and NR phase and amplitude appear to agree well until just before the PN approximant diverges. The horizontal line in the frequency plot indicates the point at which $M\omega = 0.1$; it seems reasonable to conclude that PN and NR agree fairly well up to that point. This demonstration of the qualitative agreement between NR and PN phase and amplitude mimics that performed with more care in the first published NR-PN comparison in [11]. In that work the leading PN (i.e., quadrupole) amplitude and 3.5PN TaylorT3 phase were found to agree reasonably well with the NR quantities up to about one quarter of an orbit before merger. Having observed this good qualitative agreement, we now wish to make the comparison more precise.

Detailed comparisons between PN and NR waveforms for equal-mass nonspinning low-eccentricity binaries have been reported in [12, 7, 100, 33]. It was found that most PN approximants (at 3.5PN order) predict the phase to within about a radian of the full GR result for the last 14-25 cycles before $M\omega = 0.1$, but that one approximant, TaylorT4, predicts the phase to within 0.05 rad, although this agreement is assumed to be accidental [33]. The leading quadrupole amplitude is found to disagree with

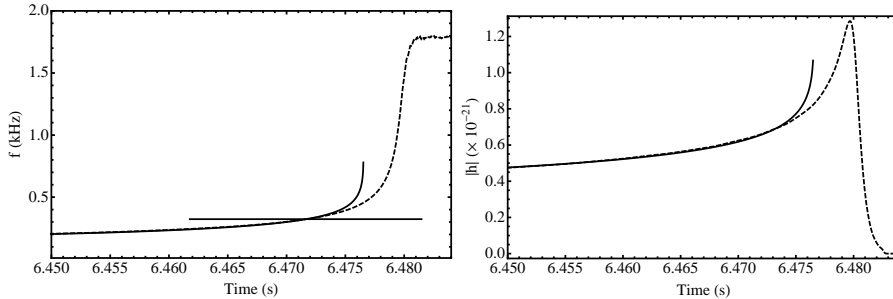


Figure 6. GW frequency and amplitude evolution for a $10 M_{\odot}$ binary starting about four orbits (eight cycles) before merger. The solid line indicates the PN values (using TaylorT1 phase and quadrupole amplitude) and the dashed line shows the NR values. The PN result is cut off just before it diverges. The results were time-shifted so that the frequencies agree at $M\omega = 0.1$, indicated by the horizontal line in the first panel.

NR results by about 6%, the 2.5PN amplitude disagrees by about 2%, and the 3PN amplitude disagrees by less than 1% [7, 33].

NR-PN comparisons moved beyond the equal-mass nonspinning case in [15], where spinning binaries were studied. The black holes had equal mass and equal spin, with the spin parallel to the orbital angular momentum of the binary. The spins considered were $a/m \sim \{0, 0.25, 0.5, 0.75, 0.85\}$. Phase comparisons were performed against the TaylorT1, T4 and Et approximants. The impressive phase accuracy of the T4 approximant was found to quickly deteriorate in the spinning case, and for black holes with spins of $a/m \sim 0.85$, the phase disagreement over the ten cycles up to $M\omega = 0.1$ was ~ 2 rad. The TaylorT1 approximant performed most consistently for all values of spin, and the largest phase disagreement was less than 1.5 rad in the highest-spin case.

When the spins are aligned parallel (or anti-parallel) to the orbital angular momentum, they remain constant throughout the evolution. In other cases the spins precess. A binary with precessing spins was studied in [22]; the mass ratio was $q = 0.8$ and the spins were $a_1 \sim 0.6$ and $a_2 \sim 0.4$. The authors compared their numerical results with PN waveforms constructed from the orbital motion predicted by an integration of the PN equations of motion, and found that the phase agreed within about 4 rad over ~ 10 cycles before merger, for the $(\ell = 2, m = 2)$ mode, although the details of the comparison make it difficult to directly compare with the published equal-mass PN-NR comparisons.

The example of the TaylorT4 approximant illustrates that the performance of a given PN approach may vary dramatically between black-hole-binary configurations. One way to test the robustness of a PN method is to examine not the final prediction of the GW phase and amplitude, but the ingredients that go into the calculation, the energy flux F and derivative of the center-of-mass energy $dE/d\omega$. These were studied for equal-mass nonspinning binaries in [101]. The authors found that none of the Taylor PN approximants predicted a flux that agreed well with NR results over the last 25 cycles before merger from an equal-mass nonspinning binary, providing further evidence that the good agreement of various PN approximants for differing black-hole-binary configurations is indeed accidental (see Fig. 9 in [101]). In contrast, effective-one-body (EOB) and Padé-resummed approximants accurately predicted both F and

$dE/d\omega$, suggesting that although these approaches do not predict the phase in the equal-mass nonspinning case as well as the TaylorT4 approximant, the EOB and Padé methods may be more robust when applied to other configurations. This prediction remains to be tested.

For the configurations for which NR and PN results have been compared, however, all of the standard approximants appear to perform adequately enough that we can move on to the question of connecting them to produce complete waveforms, which I will discuss in the next section.

5. Complete waveforms for GW searches

One way to produce complete waveforms that cover an arbitrary portion of the inspiral, plus the merger and ringdown, is to connect NR and PN waveforms to produce hybrid waveforms. A method to do this was first suggested in [99] and later in [102, 20, 103].

In [99] PN waveforms computed using a 3.5PN phase and quadrupole amplitude are matched with NR results for an equal-mass nonspinning binary. A matching frequency is chosen, and at that frequency a phase shift is applied so that the phase is continuous through the PN-NR connection. There is an amplitude difference of $\sim 10\%$ between the PN and NR waveforms (consistent with a 10% uncertainty in the NR amplitude and later calculations of the 6% error in the quadrupole amplitude), but the resulting discontinuity is removed from the hybrid-waveform amplitude by an appropriate rescaling of the PN component. The matching is performed about 12 cycles before merger.

In [102, 20, 103] a different procedure was applied. PN waveforms modeled with the TaylorT1 3.5PN phase and quadrupole amplitude were matched with NR waveforms with mass ratios $q = M_1/M_2 \in [1, 4]$, either with a spacing of $\delta q = 0.1$ using short waveforms that include only ~ 4 cycles before merger [102], or $\delta q = 1$, which include > 10 cycles before merger [20]. The matching is done not at a single frequency, but within a time interval, as follows. Consider the NR waveform over some time interval, $t \in [t_1, t_2]$. Now take a PN waveform with the same physical parameters (in this case, the mass ratio is the distinguishing parameter), and align the time and phase of the PN waveform such that the quantity

$$\delta = \int_{t_1}^{t_2} |\mathbf{h}^{PN}(t) - a\mathbf{h}^{NR}(t)|^2 dt, \quad (3)$$

is minimized. (The constant a is an amplitude scale factor, and the minimization is also performed over a .) Once the PN and NR waveforms have been aligned by this procedure, the hybrid waveform is constructed by linearly interpolating between \mathbf{h}^{PN} and \mathbf{h}^{NR} over the time interval (t_1, t_2) .

A related procedure is applied in [104], where a hybrid equal-mass nonspinning waveform is used to assess the quality of the 2PN stationary-phase-approximation (SPA) templates currently used in LIGO searches. Since current PN templates are cut off before merger, they are expected to be appropriate only for searches of binaries with a total mass above $\sim 25 M_\odot$ (see, for example [105]). The authors reach the interesting conclusion that current templates can be used to detect binaries with much higher masses if the value of the symmetric mass ratio $\eta = q/(1+q)^2$ is extended up to unphysical values, $\eta \leq 1$.

In most of the work I have described, NR and PN results were matched between about eight and ten cycles before merger. In Sec. 4 we saw how accurate various PN

approximants are in this regime, but what does this accuracy mean for GW detection? By definition we have no full GR prediction for the PN part of the hybrid waveform; if we did we would not need PN theory. The only way to assess the accuracy of the hybrid waveforms is to compare hybrid waveforms produced by different PN approximants at different PN orders. This was done in [99] by calculating the mismatch between hybrid waveforms produced using the Taylor approximants at 3PN and 3.5PN order, and between 3.5PN Taylor and EOB waveforms. If the difference between 3.5PN Taylor- and EOB-based hybrids is indicative of their *physical* error, then these hybrid waveforms are accurate enough for detection of binaries down to $10 M_{\odot}$ with the Initial LIGO, Advanced LIGO and Virgo detectors. If, however, it is the difference between 3PN and 3.5PN Taylor-based hybrids that we should pay attention to, then current hybrid waveforms are only useful down to about $20 M_{\odot}$, or $30 M_{\odot}$ in the case of Virgo, which has the broadest frequency range. (See Figs. 5 and 6 in [99].)

Combining the results in [99] with those of the Samurai analysis (Sec. 3.2), we see that the accuracy of hybrid waveforms is dictated by the accuracy of the PN or EOB ingredients. For this reason the physical accuracy of different PN approaches deserves closer attention in the future.

The construction of hybrid waveforms solves one problem in producing GW template banks: we now have waveforms of arbitrary length. Now we need to produce waveforms for *any* black-hole-binary configuration. One way to achieve this is to devise a general analytic ansatz for full waveforms, and then use the known hybrid waveforms as input to determine the unknown coefficients in the ansatz. Such “phenomenological” waveforms have been produced for unequal-mass nonspinning binaries with $q \in [1, 4]$ [102, 20, 103].

The phenomenological ansatz used in [102, 20, 103] is written in the frequency domain, and takes the form

$$u(f) \equiv \mathcal{A}_{\text{eff}}(f) e^{i\Psi_{\text{eff}}(f)}. \quad (4)$$

The effective amplitude $\mathcal{A}_{\text{eff}}(f)$ is made up of three piecewise functions: the PN quadrupole amplitude, which is proportional to $f^{-7/6}$ in the frequency domain, an empirically determined $f^{-2/3}$ behaviour during plunge and merger [11], and finally a Lorentzian is used to capture the general features of the ringdown. The effective phase $\Psi_{\text{eff}}(f)$ is written as a power series in the frequency.

There are four free parameters in the amplitude ansatz and six in the phase ansatz. The set of physical systems that are modeled by this procedure (i.e., unequal-mass nonspinning binaries) are parametrized by only two parameters (the total mass M and the mass ratio q), but the ten parameters in the phenomenological ansatz can be mapped to the two physical parameters by simple quadratic fits. This is an important result. It demonstrates that the waveforms (written in terms of this particular phenomenological ansatz) vary only slowly as the mass ratio is changed, and that the phenomenological waveform family generated from 31 short simulations separated by $\delta q = 0.1$ can be produced just as well from as few as three simulations (i.e., the number of data points needed to fit a quadratic). This allowed the accuracy of the waveform family to be substantially improved by generating four much longer (> 10 cycles) waveforms with mass ratios $q = \{1, 2, 3, 4\}$.

An entirely different procedure to produce accurate analytic waveforms is based on the effective-one-body (EOB) approach. The original EOB method [106, 107, 108, 109, 110] predicted waveforms through merger and ringdown before full numerical simulations were possible, but, despite the compelling case made for the various

physical ingredients in the EOB method, there was no way to assess the accuracy of its predictions without full GR results to compare with.

In the EOB approach the post-Newtonian description of the orbital dynamics is mapped to an *effective-one-body* description that incorporates knowledge of the test-mass limit through a resummation of the post-Newtonian GW energy and flux. This leads to an effective background metric, in which some terms are further resummed by Padé methods, motivated by physical arguments [111]. The resulting inspiral waveforms are matched to ringdown modes to produce an approximation to the complete inspiral-merger-ringdown waveform.

Numerical-relativity results have been used to calibrate and enhance EOB methods in a number of ways. A higher-order 4PN term can be added to the EOB Hamiltonian and/or flux, and the coefficient(s) fit to numerical data, first applied in [19], and later [112, 113, 114, 115, 116], or some of the existing coefficients in the EOB prescription can also be fit to numerical data [112, 113, 114, 115, 116]. Improved matching to the ringdown waveform has also been explored [112, 113, 114, 21, 116]. One may suspect that these efforts consist of successively introducing more parameters until an accurate fit is found. Instead it has been shown in these works that fitting some EOB coefficients to only equal-mass nonspinning data then leads to an accurate prediction of the results for unequal-mass binaries [114, 115, 116], and that the EOB prescription can be modified to allow accurate fits to numerical data with only a small number of free parameters [117, 115, 116].

Ultimately, one can view the EOB procedure as another form of phenomenological ansatz. The ingredients in the EOB method are all physically motivated, but so too is the form of the ansatz used in [102, 20, 103]. In the end it is quite reasonable to expect that there exist many different analytic fits to the full GR waveforms, all of which agree with each other within the uncertainties in the numerical data or the low-frequency PN ingredients. The method eventually used to produce templates for GW searches may depend on which is simpler to implement or, more likely, historical accident. A more fruitful approach may be to implement several families of template banks, which allow precise error checking and comparisons, and may allow those analyzing detector data to more quickly determine the validity of a detection.

6. Future issues

This review has focussed on the configurations of black-hole-binary systems that have been numerically simulated through at least five orbits before merger and ringdown, and efforts to quantify the accuracy of those simulations, compare them with PN results, and to combine NR and PN results to produce waveforms of arbitrary length and phenomenological waveforms that could eventually be used to accurately map the entire parameter space of black-hole-binary waveforms.

Before this is done, many more numerical waveforms will be needed. This is a large computational undertaking, and in this final section I will summarize a few of the issues that numerical relativists face in producing these simulations.

Accuracy of simulations. Current numerical simulations appear to be accurate enough for most detection and parameter-estimation purposes with current ground-based detectors [88], at least for nonspinning binaries. By this I mean that the portion of the full inspiral-merger-ringdown waveform produced numerically for a given configuration appears to be sufficiently accurate — whether *enough* of the full waveform was produced is a different question, which I discuss below. However, once

the Advanced LIGO detector comes online (around 2013) it is expected to be 10-15 times more sensitive than current detectors, and as such the accuracy requirements of waveforms (in particular for parameter estimation) will increase. A further increase in accuracy will be necessary to exploit the full scientific potential of detections from the planned space-based detector LISA (2018+) [118]. However, the accuracy requirements of numerical waveforms have not yet been established for applications with each of these detectors, and it is important that they are: not only do we wish to produce waveforms that are accurate enough, but we don't want to expend extra effort to produce results that are more accurate than required — particularly at the expense of covering more of the black-hole-binary parameter space.

There are two main issues in discussing waveform accuracy. One is the accuracy of the numerical results from the code. The other is the physical accuracy of the results, particularly the waveform extraction. It is the latter (and *not* numerical accuracy) that appears to be the main current bottleneck in improving accuracy, in particular for higher modes, which will be important for more exotic areas of the parameter space (see for example [119, 22]), and for more accurate parameter estimation (see [120, 121] for examples of estimating the sky location with LISA).

Length of simulations. A second issue, alluded to above, is whether current simulations are long enough, i.e., include enough inspiral cycles. If we wish to use exclusively numerical waveforms as search templates, then we have already seen that the simulations need to be hundreds or thousands of cycles longer — but few advocate such a severe approach. If we are to instead connect NR and PN waveforms, as discussed earlier, then we need to determine that PN waveforms are sufficiently accurate up to the point where they are matched to NR waveforms. This is difficult to establish, because we have no full GR solution to compare against, and if we did, then we could use that to match even more cycles before merger. The most fruitful approach is probably to compare different PN approximants and approaches up to the point where the PN waveform would no longer be used. This is a topic that deserves greater attention; most studies of NR waveforms prior to the success of NR simulations focussed on the faithfulness of templates that used NR waveforms all the way up to the point where each PN approximant diverges (see [122] for a recent example). This grossly over-estimates the discrepancy between PN waveforms that are cut off five, or ten, or more cycles before the standard cutoff frequency.

Higher mass ratios. The highest mass ratio binary for which full GR numerical results have been published is $q = 10$ [123]. Although the simulations include only about three orbits before merger, they are far more computationally expensive than equivalent equal-mass simulations. The finest resolution of the simulation is defined by the smallest mass, while the overall size of the binary is defined by the total mass. This means that the computational cost will scale *at best* with the mass ratio q . In practice one must usually provide greater resolution to resolve the dynamics of an unequal-mass system, meaning that we use a greater number of points on the computational domain. As such, a 10-orbit simulation of a $q = 2$ system that takes six weeks (as in the simulations used in [20, 103, 114]) will take at least fifteen months if repeated for $q = 20$, and could well take twice that long. Bear in mind that clean error estimates require a convergence series of at least three simulations, and that we really want waveforms for mass ratios up to $q = 100$ or $q = 1000$, or however far we need to go to make a conclusive connection to the extreme-mass-ratio regime of perturbation theory, and it becomes clear that we require either phenomenal computer resources, or a serious advance in numerical methods. Exploration of alternative

numerical integration methods [124] are a first step in this direction, although it is likely that more radical approaches are required, and that the real solution of this problem will represent a breakthrough comparable to the first successful black-hole-binary simulations in 2005.

High-mass-ratio simulations for $q > 100$ are impractical at present, but this situation could quickly change with improvements in the formulation of the problem, numerical methods and computer hardware. Order-of-magnitude improvements in either code speed, accuracy or memory efficiency are common when new numerical methods are introduced. As an example in the opposite direction, if current typical mesh-refinement simulations were performed on a uniform grid, the memory requirements would be millions of times larger. Full black-hole-binary simulations have been possible for only a few years, and the possibilities for improving on current methods are only beginning to be explored.

Acknowledgments

This work was supported by SFI grant 07/RFP/PHYF148, and I thank the Albert Einstein Institute, Potsdam, for hospitality. I am grateful to Sascha Husa and Niall Ó Murchadha for many useful discussions, and for a careful reading of the manuscript.

References

- [1] Abramovici A A, Althouse W, Drever R P, Gursel Y, Kawamura S, Raab F, Shoemaker D, Sievers L, Spero R, Thorne K S, Vogt R, Weiss R, Whitcomb S and Zuker M 1992 *Science* **256** 325–333
- [2] Acernese F *et al.* 2006 *Class. Quantum Grav.* **23** S635–S642
- [3] Hild (for the LIGO Scientific Collaboration) S 2006 *Class. Quantum Grav.* **23** S643–S651
- [4] Pretorius F 2005 *Phys. Rev. Lett.* **95** 121101 (*Preprint gr-qc/0507014*)
- [5] Campanelli M, Lousto C O, Marronetti P and Zlochower Y 2006 *Phys. Rev. Lett.* **96** 111101 (*Preprint gr-qc/0511048*)
- [6] Baker J G, Centrella J, Choi D I, Koppitz M and van Meter J 2006 *Phys. Rev. Lett.* **96** 111102 (*Preprint gr-qc/0511103*)
- [7] Hannam M, Husa S, González J A, Sperhake U and Brüggmann B 2008 *Phys. Rev. D* **77** 044020 (*Preprint arXiv:0706.1305[gr-qc]*)
- [8] Adhikari R, Fritschel P and Waldman S 2006 Enhanced ligo Tech. Rep. LIGO-T060156-01-I LIGO Scientific Collaboration <http://www.ligo.caltech.edu/docs/T/T060156-01.pdf>
- [9] Campanelli M, Lousto C O and Zlochower Y 2006 *Phys. Rev. D* **73** 061501(R) (*Preprint gr-qc/0601091*)
- [10] Baker J G, Centrella J, Choi D I, Koppitz M and van Meter J 2006 *Phys. Rev. D* **73** 104002 (*Preprint gr-qc/0602026*)
- [11] Buonanno A, Cook G B and Pretorius F 2007 *Phys. Rev. D* **75** 124018 (*Preprint gr-qc/0610122*)
- [12] Baker J G, van Meter J R, McWilliams S T, Centrella J and Kelly B J 2007 *Phys. Rev. Lett.* **99** 181101 (*Preprint gr-qc/0612024*)
- [13] Scheel M A *et al.* 2008 (*Preprint 0810.1767*)
- [14] Flanagan E E and Hughes S 1998 *Phys. Rev. D* **57** 4535
- [15] Hannam M, Husa S, Brüggmann B and Gopakumar A 2008 *Phys. Rev. D* **78** 104007 (*Preprint 0712.3787*)
- [16] Hinder I, Herrmann F, Laguna P and Shoemaker D 2008 (*Preprint 0806.1037*)
- [17] Sperhake U *et al.* 2008 *Phys. Rev. D* **78** 064069 (*Preprint 0710.3823*)
- [18] Dain S, Lousto C O and Zlochower Y 2008 *Phys. Rev. D* **78** 024039 (*Preprint 0803.0351*)
- [19] Buonanno A *et al.* 2007 *Phys. Rev. D* **76** 104049 (*Preprint 0706.3732*)
- [20] Ajith P *et al.* 2008 *Phys. Rev. D* **77** 104017 (*Preprint 0710.2335*)
- [21] Baker J G *et al.* 2008 *Phys. Rev. D* **78** 044046 (*Preprint 0805.1428*)
- [22] Campanelli M, Lousto C O, Nakano H and Zlochower Y 2008 (*Preprint 0808.0713*)

- [23] Alcubierre M 2008 *Introduction to 3+1 Numerical Relativity* (USA: Oxford University Press) ISBN 978-0199205677
- [24] Pretorius F 2007 (*Preprint* 0710.1338)
- [25] Berger M J and Oliger J 1984 *J. Comput. Phys.* **53** 484–512
- [26] Campanelli M, Lousto C O and Zlochower Y 2006 *Phys. Rev. D* **74** 041501(R) (*Preprint* gr-qc/0604012)
- [27] Campanelli M, Lousto C O and Zlochower Y 2006 *Phys. Rev. D* **74** 084023 (*Preprint* gr-qc/0608275)
- [28] Campanelli M, Lousto C O, Zlochower Y and Merritt D 2007 *Astrophys. J.* **659** L5–L8 (*Preprint* gr-qc/0701164)
- [29] Etienne Z B, Faber J A, Liu Y T, Shapiro S L and Baumgarte T W 2007 *Phys. Rev.* **D76** 101503 (*Preprint* arXiv:0707.2083[gr-qc])
- [30] Scheel M A *et al.* 2006 *Phys. Rev.* **D74** 104006 (*Preprint* gr-qc/0607056)
- [31] Pretorius F 2005 *Class. Quantum Grav.* **22** 425–452 (*Preprint* gr-qc/0407110)
- [32] Rinne O, Lindblom L and Scheel M A 2007 *Class. Quant. Grav.* **24** 4053–4078 (*Preprint* 0704.0782)
- [33] Boyle M *et al.* 2007 *Phys. Rev.* **D76** 124038 (*Preprint* 0710.0158)
- [34] Aylott B *et al.* 2009 (*Preprint* 0901.4399)
- [35] Thornburg J 1987 *Class. Quantum Grav.* **4**(5) 1119–1131 URL <http://stacks.iop.org/0264-9381/4/1119>
- [36] Pretorius F 2006 *Class. Quantum Grav.* **23** S529–S552 (*Preprint* gr-qc/0602115)
- [37] York J W 1999 *Phys. Rev. Lett.* **82** 1350–1353
- [38] Pfeiffer H P and York J W 2003 *Phys. Rev. D* **67** 044022 (*Preprint* gr-qc/0207095)
- [39] Cook G B 2002 *Phys. Rev. D* **65** 084003 (*Preprint* gr-qc/0108076)
- [40] Cook G B and Pfeiffer H P 2004 *Phys. Rev. D* **70** (*Preprint* gr-qc/0407078)
- [41] Caudill M, Cook G B, Grigsby J D and Pfeiffer H P 2006 *Phys. Rev. D* **74** 064011 (*Preprint* gr-qc/0605053)
- [42] Beig R and O’Murchadha N 1994 *Class. Quantum Grav.* **11** 419
- [43] Beig R and Husa S 1994 *Phys. Rev. D* **50** R7116–7118 (*Preprint* gr-qc/9410003)
- [44] Dain S and Friedrich H 2001 *Comm. Math. Phys.* **222** 569 gr-qc/0102047
- [45] Brandt S and Brüggmann B 1997 *Phys. Rev. Lett.* **78**(19) 3606–3609 (*Preprint* gr-qc/9703066)
- [46] Hannam M, Husa S, Ohme F, Brüggmann B and O’Murchadha N 2008 *Phys. Rev. D* **78** 064020 (*Preprint* 0804.0628)
- [47] Hannam M, Husa S, Pollney D, Brüggmann B and Ó Murchadha N 2007 *Phys. Rev. Lett.* **99** 241102 gr-qc/0606099
- [48] Hannam M, Husa S, Ó Murchadha N, Brüggmann B, González J A and Sperhake U 2007 *Journal of Physics: Conference series* **66** 012047 (*Preprint* arXiv:gr-qc/0612097)
- [49] Brown J D 2008 *Phys. Rev.* **D77** 044018 (*Preprint* arXiv:0705.1359[gr-qc])
- [50] Dain S, Lousto C O and Takahashi R 2002 *Phys. Rev. D* **65** 104038 (*Preprint* gr-qc/0201062)
- [51] Sperhake U, Cardoso V, Pretorius F, Berti E and Gonzalez J A 2008 *Phys. Rev. Lett.* **101** 161101 (*Preprint* 0806.1738)
- [52] Shibata M, Okawa H and Yamamoto T 2008 *Phys. Rev.* **D78** 101501 (*Preprint* 0810.4735)
- [53] Matzner R A, Huq M F and Shoemaker D 1999 *Phys. Rev. D* **59** 024015
- [54] Marronetti P, Huq M F, Laguna P, Lehner L, Matzner R A and Shoemaker D 2000 *Phys. Rev. D* **62** 024017 gr-qc/0001077
- [55] Marronetti P and Matzner R A 2000 *Phys. Rev. Lett.* **85** 5500–5503 gr-qc/0009044
- [56] Bonning E, Marronetti P, Neilsen D and Matzner R 2003 *Phys. Rev.* **D68** 044019
- [57] Lovelace G, Owen R, Pfeiffer H P and Chu T 2008 (*Preprint* 0805.4192)
- [58] Lovelace G 2008 (*Preprint* 0812.3132)
- [59] Cook G B and Baumgarte T W 2008 *Phys. Rev.* **D78** 104016 (*Preprint* 0810.4493)
- [60] Hannam M, Husa S, Brüggmann B, Gonzalez J A and Sperhake U 2007 *Class. Quantum Grav.* **24** S15–S24 (*Preprint* arXiv:gr-qc/0612001)
- [61] Kelly B J, Tichy W, Campanelli M and Whiting B F 2007 *Phys. Rev.* **D76** 024008 (*Preprint* 0704.0628)
- [62] Friedrich H and Rendall A D 2000 *Lect. Notes Phys.* **540** 127–224 (*Preprint* gr-qc/0002074)
- [63] Husa S 2007 *Eur. Phys. J. ST* **152** 183–207 (*Preprint* 0812.4395)
- [64] Alcubierre M, Allen G, Bona C, Fiske D, Goodale T, Guzmán F S, Hawke I, Hawley S H, Husa S, Koppitz M, Lechner C, Pollney D, Rideout D, Salgado M, Schnetter E, Seidel E, aki Shinkai H, Szilagy B, Shoemaker D, Takahashi R and Winicour J 2004 *Class. Quantum Grav.* **21** 589 (*Preprint* gr-qc/0305023)
- [65] Babiuc M C *et al.* 2008 *Class. Quant. Grav.* **25** 125012 (*Preprint* 0709.3559)

- [66] Friedrich H 1985 *Comm. Math. Phys.* **100** 525–543
- [67] Lindblom L, Scheel M A, Kidder L E, Owen R and Rinne O 2006 *Class. Quantum Grav.* **23** S447–S462 (*Preprint gr-qc/0512093*)
- [68] Shibata M and Nakamura T 1995 *Phys. Rev. D* **52** 5428
- [69] Baumgarte T W and Shapiro S L 1998 *Phys. Rev. D* **59** 024007 (*Preprint gr-qc/9810065*)
- [70] Szilagyi B, Pollney D, Rezzolla L, Thornburg J and Winicour J 2007 *Class. Quant. Grav.* **24** S275–S293 (*Preprint gr-qc/0612150*)
- [71] Arnowitt R, Deser S and Misner C W 1962 in L Witten, ed, *Gravitation an introduction to current research* (John Wiley, New York) pp 227–265 *gr-qc/0405109*
- [72] York J W 1979 in L L Smarr, ed, *Sources of gravitational radiation* (Cambridge, UK: Cambridge University Press) pp 83–126 ISBN 0-521-22778-X
- [73] Marronetti P, Tichy W, Brüggmann B, González J and Spherhake U 2008 *Phys. Rev. D* **77** 064010 (*Preprint arXiv:0709.2160[gr-qc]*)
- [74] van Meter J R, Baker J G, Koppitz M and Choi D I 2006 *Phys. Rev. D* **73** 124011 (*Preprint gr-qc/0605030*)
- [75] Gundlach C and Martin-Garcia J M 2006 *Phys. Rev. D* **74** 024016 (*Preprint gr-qc/0604035*)
- [76] Newman E T and Penrose R 1962 *J. Math. Phys.* **3**(3) 566–578 erratum in *J. Math. Phys.* **4**, 998 (1963)
- [77] Stewart J M 1990 *Advanced general relativity* (Cambridge, England: Cambridge University Press)
- [78] Nagar A and Rezzolla L 2005 *Class. Quantum Grav.* **22** R167 (*Preprint gr-qc/0502064*)
- [79] Lehner L and Moreschi O M 2007 *Phys. Rev.* **D76** 124040 (*Preprint 0706.1319*)
- [80] Koppitz M *et al.* 2007 *Phys. Rev. Lett.* **99** 041102 (*Preprint gr-qc/0701163*)
- [81] Husa S 2008 Exploring the usefulness of numerical waveforms for data analysis talk given at NRDA meeting, Syracuse URL <https://www.gravity.phy.syr.edu/dokuwiki/doku.php?id=unhbox\voidb0x\bgroupl\et\unhbox\voidb0x\setbox\@tempboxa\hb>
- [82] Pfeiffer H P *et al.* 2007 *Class. Quant. Grav.* **24** S59–S82 (*Preprint gr-qc/0702106*)
- [83] Husa S, Hannam M, Gonzalez J A, Spherhake U and Brüggmann B 2008 *Phys. Rev.* **D77** 044037 (*Preprint 0706.0904*)
- [84] Walther B, Bruegmann B and Mueller D 2009 (*Preprint 0901.0993*)
- [85] Husa S, Gonzalez J A, Hannam M, Brüggmann B and Spherhake U 2008 *Class. Quant. Grav.* **25** 105006 (*Preprint 0706.0740*)
- [86] Lousto C O and Zlochower Y 2008 *Phys. Rev.* **D77** 024034 (*Preprint arXiv:0711.1165[gr-qc]*)
- [87] Baker J G, Campanelli M, Pretorius F and Zlochower Y 2007 *Class. Quant. Grav.* **24** S25–S31 (*Preprint gr-qc/0701016*)
- [88] Hannam M *et al.* 2009 (*Preprint 0901.2437*)
- [89] Brüggmann B *et al.* 2008 *Phys. Rev.* **D77** 024027 (*Preprint gr-qc/0610128*)
- [90] Husa S, González J A, Hannam M, Brüggmann B and Spherhake U 2008 *Class. Quantum Grav.* **25** 105006 (*Preprint arXiv:0706.0740[gr-qc]*)
- [91] Pollney D *et al.* 2007 *Phys. Rev.* **D76** 124002 (*Preprint 0707.2559*)
- [92] Imbiriba B, Baker J, Choi D I, Centrella J, Fiske D R, Brown J D, van Meter J R and Olson K 2004 (*Preprint gr-qc/0403048*)
- [93] Vaishnav B, Hinder I, Herrmann F and Shoemaker D 2007 *Phys. Rev.* **D76** 084020 (*Preprint arXiv:0705.3829[gr-qc]*)
- [94] Scheel M A, Pfeiffer H P, Lindblom L, Kidder L E, Rinne O and Teukolsky S A 2006 *Phys. Rev. D* **74** 104006 (*Preprint gr-qc/0607056*)
- [95] Owen B J 1996 *Phys. Rev. D* **55** 6749
- [96] Lindblom L, Owen B J and Brown D A 2008 (*Preprint 0809.3844*)
- [97] Sintes A M and Vecchio A 1999 (*Preprint gr-qc/0005058*)
- [98] Van Den Broeck C and Sengupta A S 2007 *Class. Quant. Grav.* **24** 1089–1114 (*Preprint gr-qc/0610126*)
- [99] Pan Y *et al.* 2008 *Phys. Rev.* **D77** 024014 (*Preprint 0704.1964*)
- [100] Gopakumar A 2007 (*Preprint 0712.3236*)
- [101] Boyle M *et al.* 2008 *Phys. Rev.* **D78** 104020 (*Preprint 0804.4184*)
- [102] Ajith P, Babak S, Chen Y, Hewitson M, Krishnan B, Whelan J T, Brüggmann B, Diener P, González J, Hannam M, Husa S, Koppitz M, Pollney D, Rezzolla L, Santamaria L, Sintes A M, Spherhake U and Thornburg J 2007 *Class. Quantum Grav.* **24** S689–S699 (*Preprint arXiv:0704.3764[gr-qc]*)
- [103] Ajith P 2008 *Class. Quant. Grav.* **25** 114033 (*Preprint 0712.0343*)
- [104] Boyle M, Brown D A and Pekowsky L 2009 (*Preprint 0901.1628*)
- [105] Collaboration L S 2009 (*Preprint 0901.0302*)

- [106] Buonanno A and Damour T 1999 *Phys. Rev. D* **59** 084006 (*Preprint arXiv:gr-qc/9811091*)
- [107] Buonanno A and Damour T 2000 *Phys. Rev. D* **62** 064015 (*Preprint gr-qc/0001013*)
- [108] Damour T, Jaranowski P and Schäfer G 2000 *Phys. Rev. D* **62** 084011 (*Preprint gr-qc/0005034*)
- [109] Damour T 2001 *Phys. Rev. D* **64** 124013 (*Preprint gr-qc/0103018*)
- [110] Buonanno A, Chen Y and Damour T 2006 *Phys. Rev.* **D74** 104005 (*Preprint gr-qc/0508067*)
- [111] Damour T, Iyer B R and Sathyaprakash B S 1998 *Phys. Rev. D* **57** 885–907 (*Preprint gr-qc/9708034*)
- [112] Damour T and Nagar A 2008 *Phys. Rev.* **D77** 024043 (*Preprint 0711.2628*)
- [113] Damour T, Nagar A, Dorband E N, Pollney D and Rezzolla L 2008 *Phys. Rev.* **D77** 084017 (*Preprint 0712.3003*)
- [114] Damour T, Nagar A, Hannam M, Husa S and Brüggmann B 2008 *Phys. Rev.* **D78** 044039 (*Preprint 0803.3162*)
- [115] Damour T and Nagar A 2009 (*Preprint 0902.0136*)
- [116] Buonanno A *et al.* 2009 (*Preprint 0902.0790*)
- [117] Mroue A H, Kidder L E and Teukolsky S A 2008 *Phys. Rev.* **D78** 044004 (*Preprint 0805.2390*)
- [118] Danzmann K and Rüdiger A 2003 *Class. Quantum Grav.* **20** S1–S9 URL stacks.iop.org/CQG/20/S2
- [119] Berti E *et al.* 2007 *Phys. Rev.* **D76** 064034 (*Preprint gr-qc/0703053*)
- [120] Babak S, Hannam M, Husa S and Schutz B 2008 (*Preprint 0806.1591*)
- [121] Thorpe J I *et al.* 2008 (*Preprint 0811.0833*)
- [122] Bose S, Gopakumar A and Tessmer M 2008 (*Preprint 0807.2400*)
- [123] Gonzalez J A, Sperhake U and Bruegmann B 2008 (*Preprint 0811.3952*)
- [124] Lau S R, Pfeiffer H P and Hesthaven J S 2008 (*Preprint 0808.2597*)